SUPPORTING INFORMATION

Excited-state dynamics of colloidal gold nanoshells functionalized with trimethoxysilylazachalcones

Marta Gordel-Wójcik*[1,2,5], Muhammed A. Thottappali[2], Marek Pietrzak[3], Elizaveta F. Petrusevich[4], Jiří Vohlídal[5], Jiří Pfleger[2], Beata Jędrzejewska[3]

[1]Faculty of Chemistry, University of Wrocław, 14.p F. Joliot-Curie Street, 50-383, Wrocław, Poland

[2]Department of Polymers for Electronics and Photonics, Institute of Macromolecular Chemistry, Czech Academy of Sciences, Heyrovského nám. 2, 16206 Prague 6, Czech Republic

[3]Faculty of Chemical Technology and Engineering, Bydgoszcz University of Science and Technology, Seminaryjna 3, 85-326 Bydgoszcz, Poland

[4]Faculty of Chemistry, University of Gdańsk, Fahrenheit Union of Universities in Gdańsk, Wita Stwosza 63, Gdańsk 80-308 Gdańsk, Poland

[5]Department of Physical and Macromolecular Chemistry, Faculty of Science, Charles University, Prague, Czech Republic

E-mail address of corresponding author: marta.gordel-wojcik@uwr.edu.pl

Table of contents	page

Snthesis of trimethoxysilylazachalcones

General method: The appropriate azachalcone (0.80 mmol), anhydrous acetonitrile (6 mL) and (3-iodopropyl)trimethoxysilane (1.84 mmol, 0.53 g) were placed, upstream of argon into a sealed reactor equipped with a magnetic stirrer, which was sealed and heated under stirring at 80-82 ℃ for 24 h. After this time, the reactor content was cooled and evaporated to dryness, not exceeding a temperature of 45 ℃. The obtained crude product was purified by flash chromatography using dichloromethane/methanol 95/5 v/v as eluent.

4N1Si

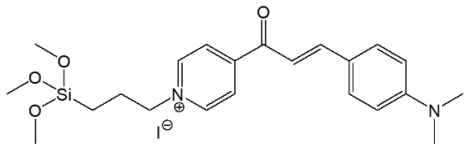

Yield: 0.221 g; 51%; 542.5 g/mol; mp 186-188 ℃; R_f = 0.54
^{1}H NMR (400 MHz, DMSO-d_6) δ (ppm): 9.27 (d, *J*=6.6 Hz, 2H), 8.63(d, *J*=6.6 Hz, 2H), 7.83 (d, *J*=15.3 Hz, 1H, -C*H*=), 7.79 (d, *J*=8.9 Hz, 2H), 7.65 (d, *J*=15.3 Hz, 1H, -C*H*=), 6.79 (d, *J*=9.0 Hz, 2H), 4.64 (t, *J*=7.2 Hz, 2H), 3.48 (s, 9H, Si(OCH_3)$_3$), 3.06 (s, 6H, N(CH_3)$_2$), 2.01 (m, 2H), 0.63 (m, 2H, Si-CH_2).
^{13}C{^{1}H} NMR (100 MHz, DMSO-d_6) δ (ppm): 185.7 (CO), 153.4, 151.5, 149.8, 146.4, 132.4, 126.5, 121.9, 115.2, 112.3, 63.3, 50.6, 40.2 (N(CH_3)$_2$), 25.2, 5.9.
HRMS (TOF MS ES+) m/z calcd. for $C_{22}H_{31}N_2O_4Si^+$ [M]$^+$, 415.2053; found, 415.2366.

4N2Si

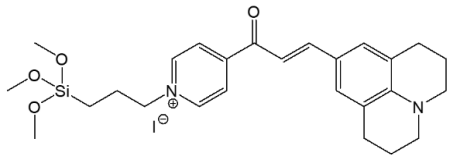

Yield: 0.198 g; 41.7%; 594.5 g/mol; mp 175-176 ℃; R_f = 0.63
^{1}H NMR (400 MHz, DMSO-d_6) δ (ppm): 9.24 (d, *J*=6.7 Hz, 2H), 8.61 (d, *J*=6.6 Hz, 2H), 7.72 (d, *J*=15.0 Hz, 1H, -C*H*=), 7.53 (d, *J*=15.0 Hz, 1H, -C*H*=), 7.34 (s, 1H), 4.62 (t, *J*=7.2Hz, 2H), 3.48 (s, 9H, Si(OCH_3)$_3$), 3.31 (t, *J*=5.8 Hz, 4H), 2.71 (t, *J*=6.0 Hz, 4H), 2.01 (m, 2H), 1.88 (t, J=5.2 Hz, 4H), 0.62 (m, 2H, Si-CH_2).
^{13}C{^{1}H} NMR (100 MHz, DMSO-d_6) δ (ppm): 184.6 (CO), 151.7, 150.1, 147.0, 146.2, 130.0, 126.3, 121.2, 120.8, 113.5, 63.2, 50.6, 49.9, 27.5, 25.2, 21.3, 5.9.
HRMS (TOF MS ES+) m/z calcd. for $C_{26}H_{35}N_2O_4Si^+$ [M + H]$^+$, 468.2444; found, 468.2476.

3N1Si

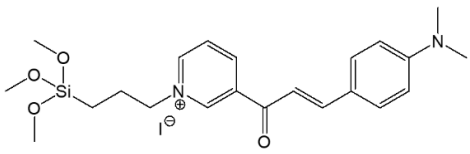

Yield: 0.201 g; 46.4%; 542.5 g/mol; mp 138-141 ℃; R_f = 0.48
^{1}H NMR (400 MHz, DMSO-d_6) δ (ppm): 9.71 (s, 1H), 9.25 (d, *J*=6.0 Hz, 1H), 9.16 (d, *J*=8.1 Hz, 1H), 8.31 (t, *J*=7.1 Hz, 1H), 7.88 (d, *J*=15.2 Hz, 1H, -C*H*=), 7.79 (d, *J*=8.9 Hz, 2H), 7.68 (d, *J*=15.2 Hz, 1H, -C*H*=), 6.79 (d, *J*=9.0 Hz, 2H), 4.68 (t, *J*=7.3 Hz, 2H), 3.48 (s, 9H, Si(OCH_3)$_3$), 3.07 (s, 6H, N(CH_3)$_2$), 2.04 (m, 2H), 0.65 (m, 2H, Si-CH_2).
^{13}C{^{1}H} NMR (100 MHz, DMSO-d_6) δ (ppm): 184.1 (CO), 153.2, 148.8, 147.1, 145.6, 144.4, 137.7, 132.2, 128.6, 121.9, 115.0, 112.2, 63.6, 50.6, 40.2 (N(CH_3)$_2$), 25.2, 5.9.
HRMS (TOF MS ES+) m/z calcd. for $C_{22}H_{31}N_2O_4Si^+$ [M]$^+$, 415.2053; found, 415.2158.

3N2Si

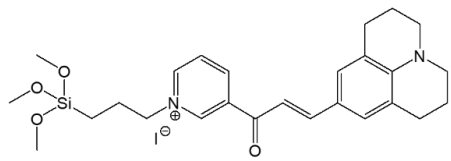

Yield: 0.197 g; 41.5%; 594.5 g/mol; mp 120-122 ℃; R_f = 0.56

^{1}H NMR (400 MHz, DMSO-d_6) δ (ppm): 9.68 (s, 1H), 9.23 (d, *J*=6.0 Hz, 1H), 9.14 (d, *J*=8.2 Hz, 1H), 8.30 (t, *J*=7.1 Hz, 1H), 7.76 (d, *J*=15.0 Hz, 1H, -CH=), 7.55 (d, *J*=15.0 Hz, 1H, -CH=), 7.34 (s, 2H), 4.67 (t, *J*=7.3 Hz, 2H), 3.48 (s, 9H, $Si(OCH_3)_3$), 3.30 (t, *J*=5.8 Hz, 4H), 2.72 (t, *J*=6.0 Hz, 4H), 2.03 (m, 2H), 1.88 (t, *J*=5.2 Hz, 4H), 0.65 (m, 2H, $Si\text{-}CH_2$).

^{13}C{^{1}H} NMR (100 MHz, DMSO-d_6) δ (ppm): 183.4 (CO), 149.2, 147.0, 146.7, 145.5, 144.2, 137.9, 129.8, 128.6, 121.1, 120.7, 113.3, 63.6, 50.6, 49.8, 27.5, 25.2, 21.3, 5.9.

HRMS (TOF MS ES+) m/z calcd. for $C_{26}H_{35}N_2O_4Si^+$ $[M + H]^+$, 468.2444; found, 468.2485.

^{1}H NMR spectrum of **4N1Si**

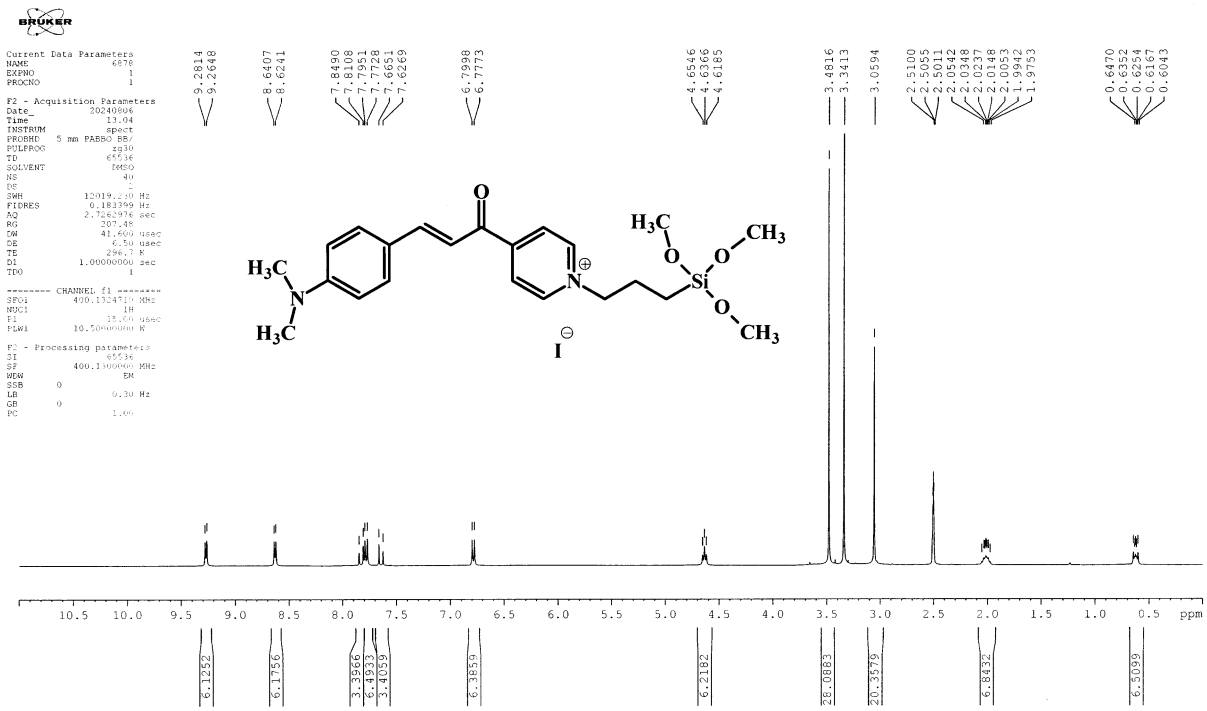

^{13}C NMR spectrum of **4N1Si**

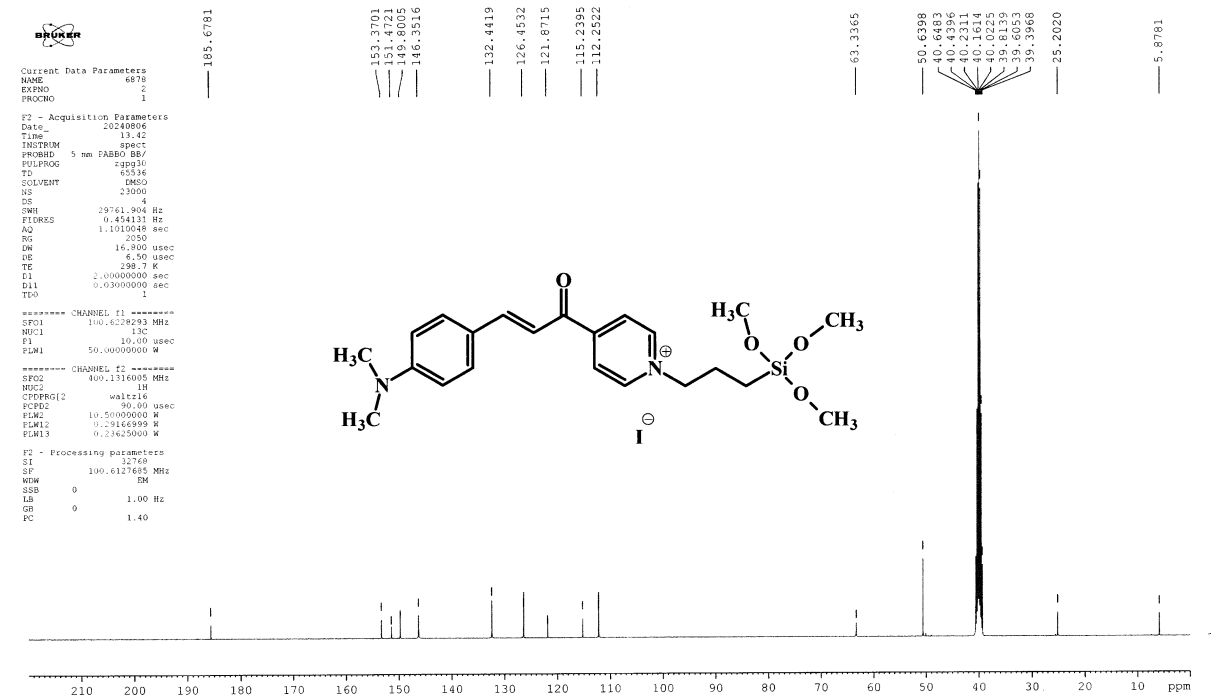

^{1}H NMR spectrum of **4N2Si**

^{13}C NMR spectrum of **4N2Si**

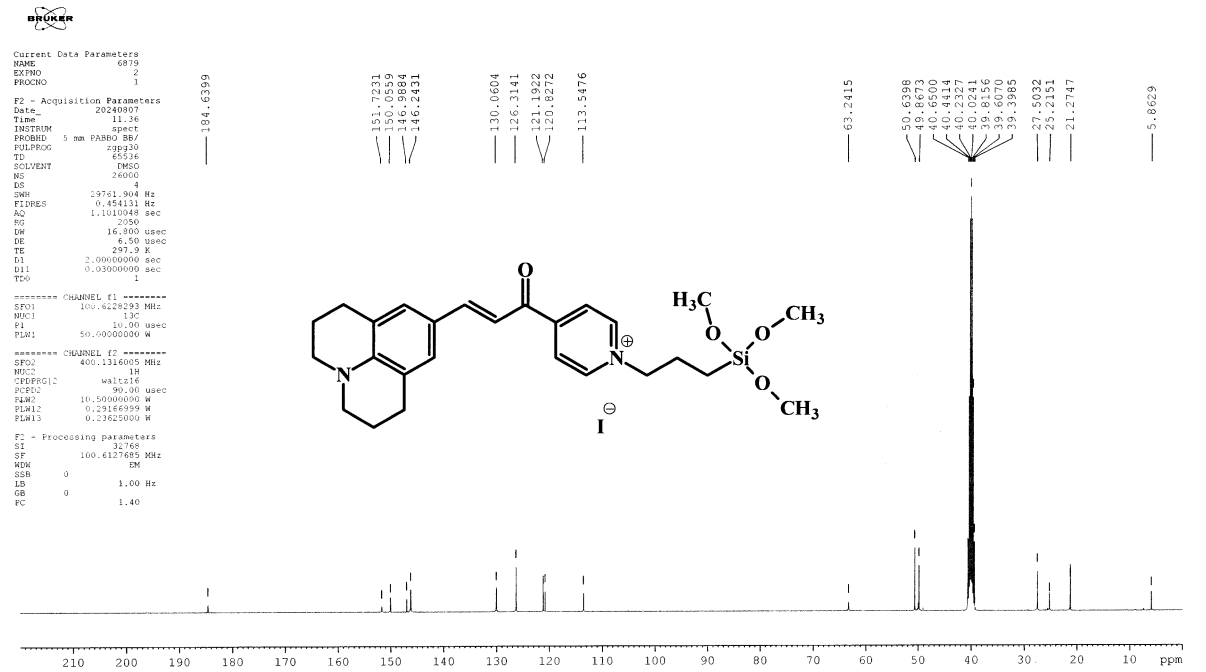

[1]H NMR spectrum of **3N1Si**

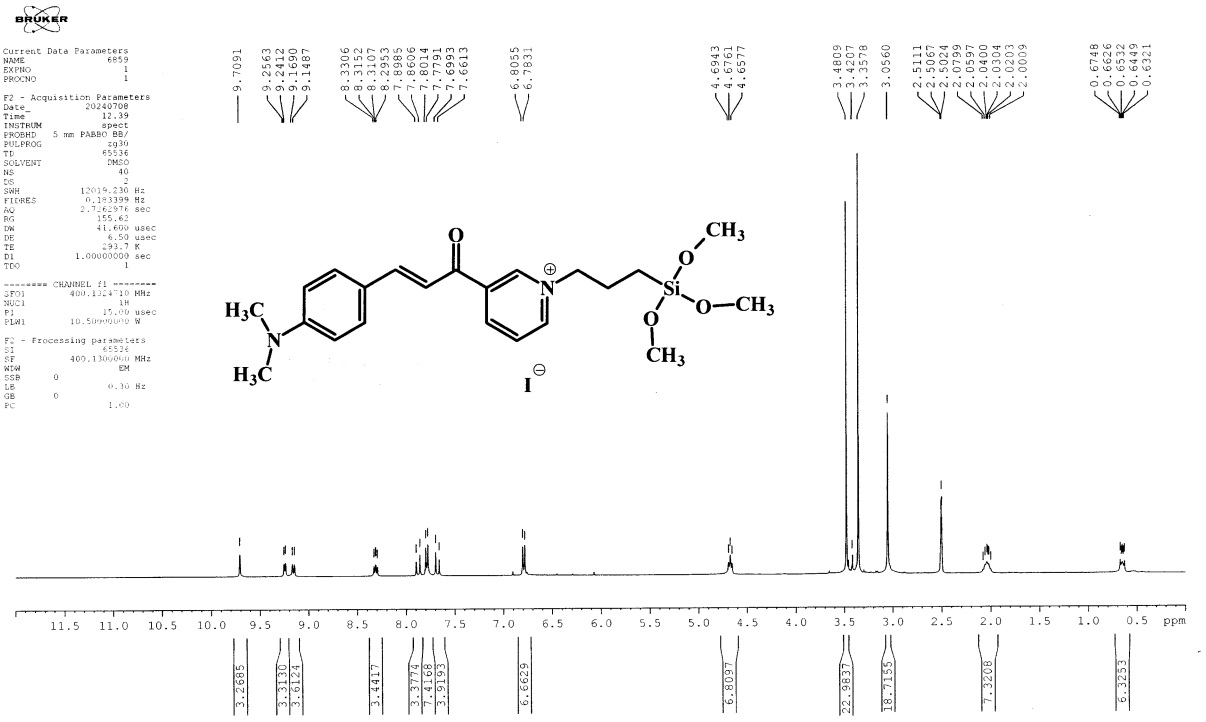

[13]C NMR spectrum of **3N1Si**

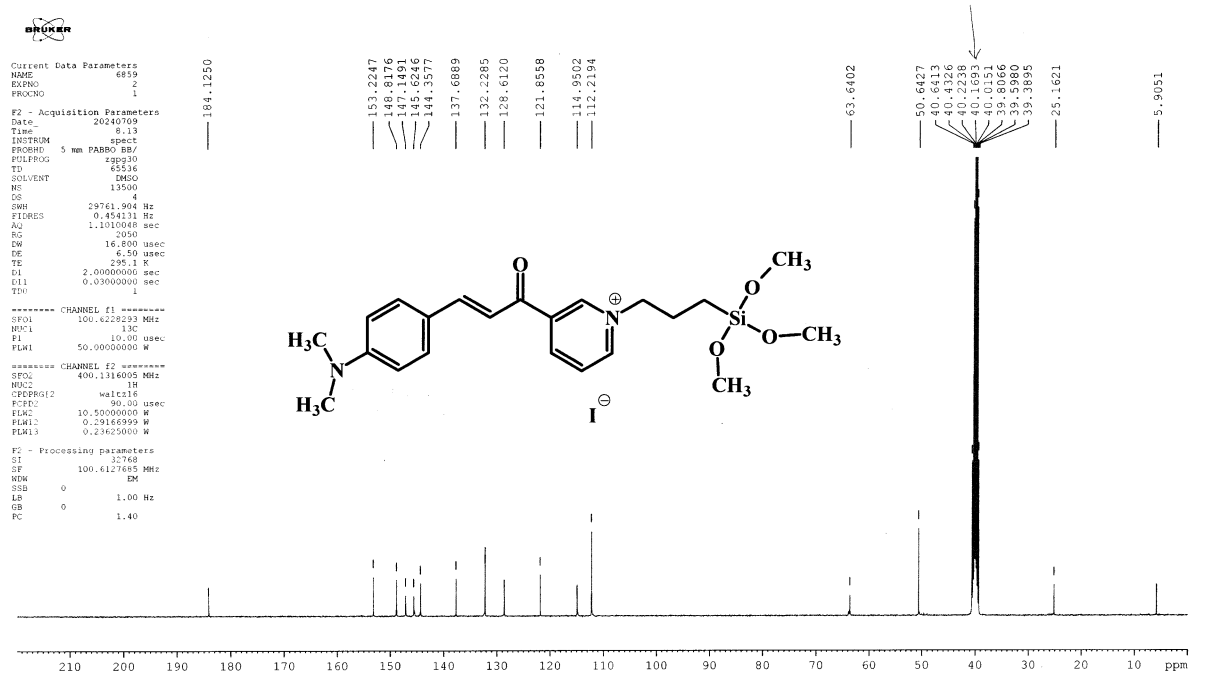

^{1}H NMR spectrum of **3N2Si**

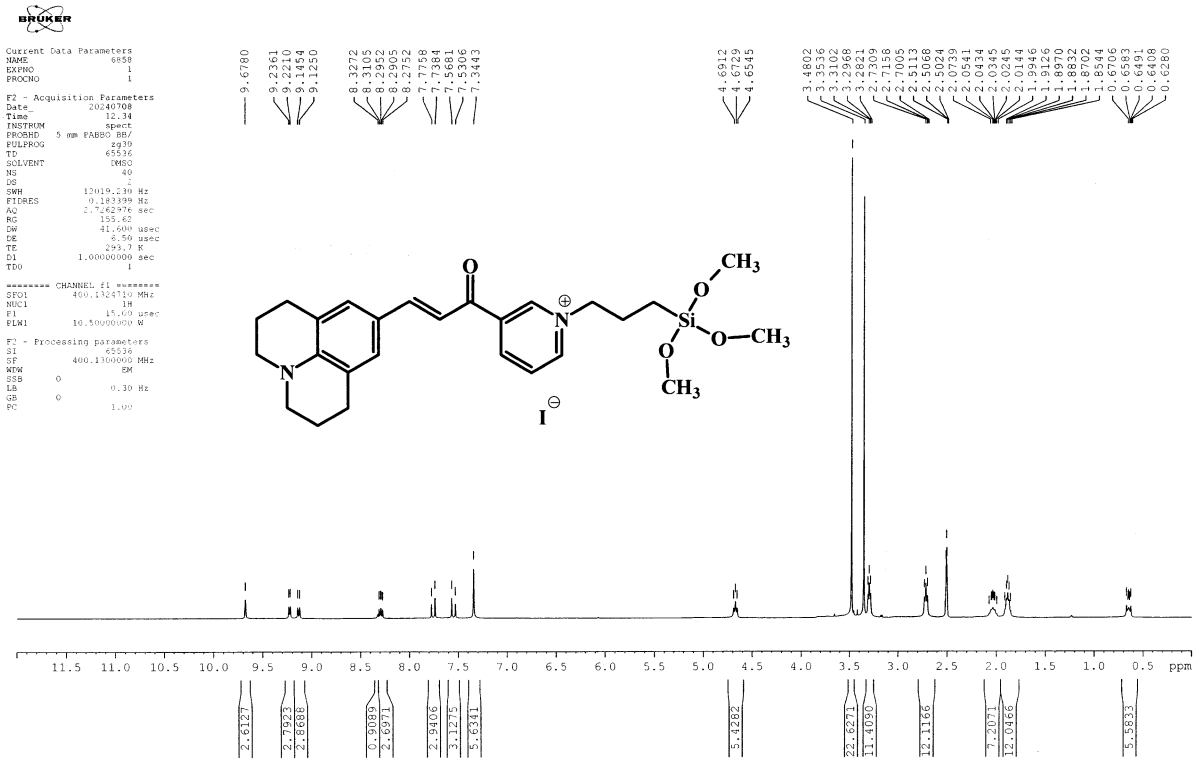

^{13}C NMR spectrum of **3N2Si**

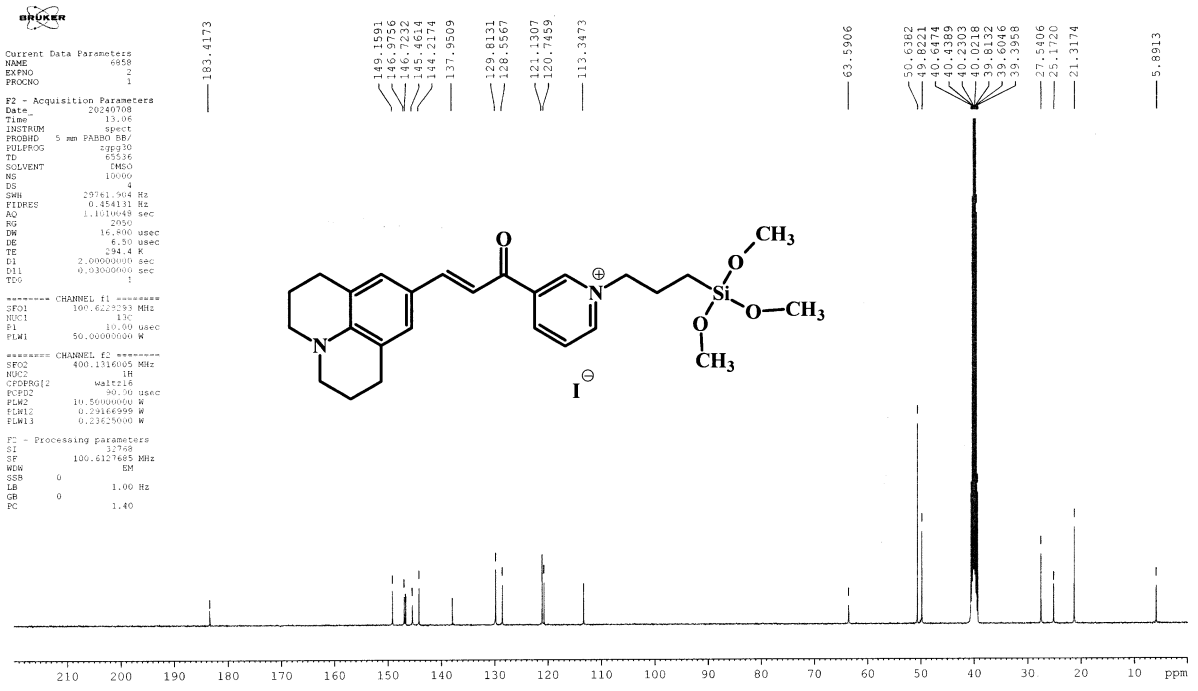

ESI(+) HRMS mass spectrum of **4N1Si** product dissolved in methanol solution.

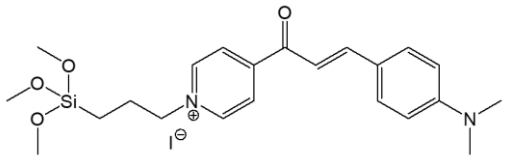

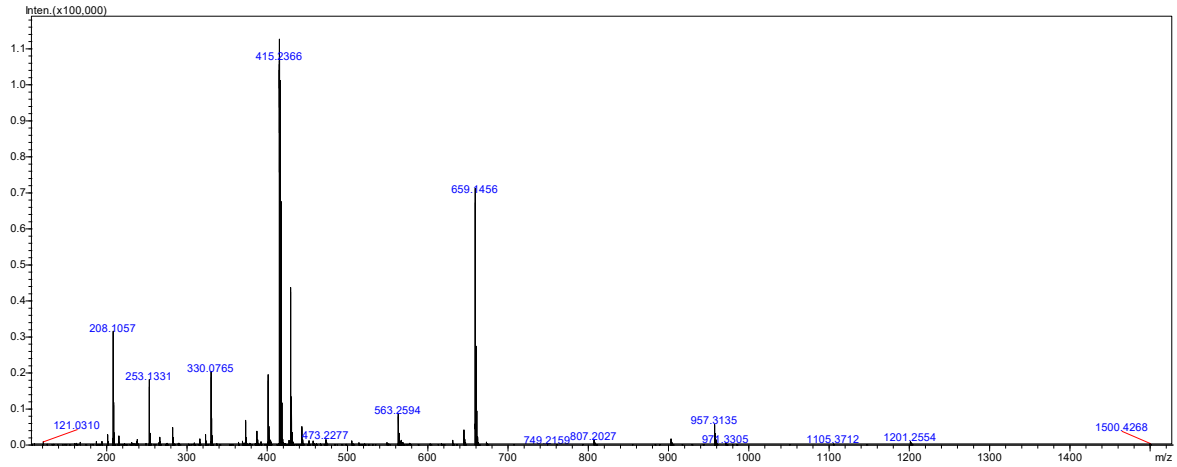

Enlarged MS spectrum in the range 375–580 m/z

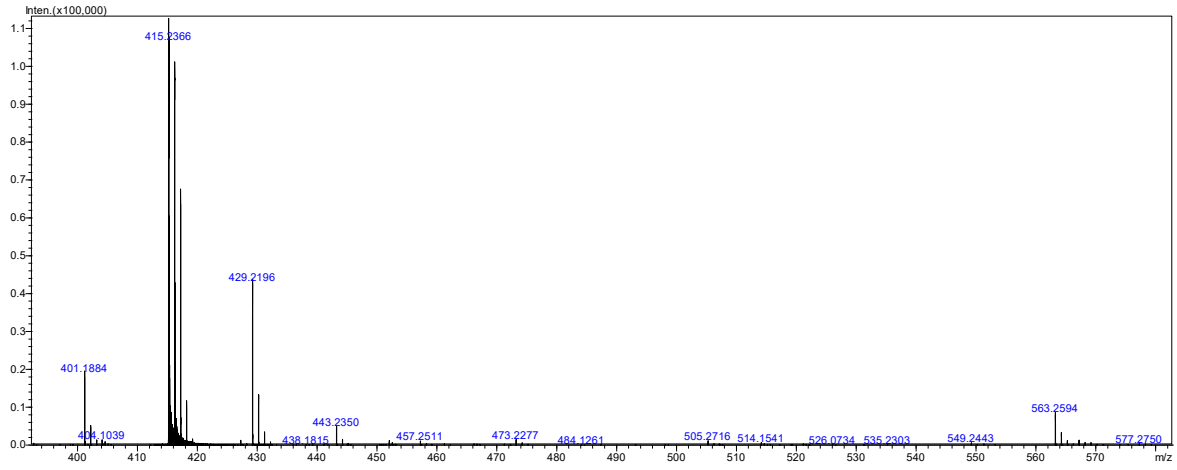

ESI(+) HRMS mass spectrum of **3N1Si** product dissolved in methanol solution.

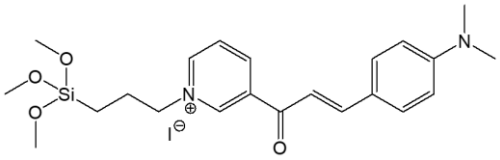

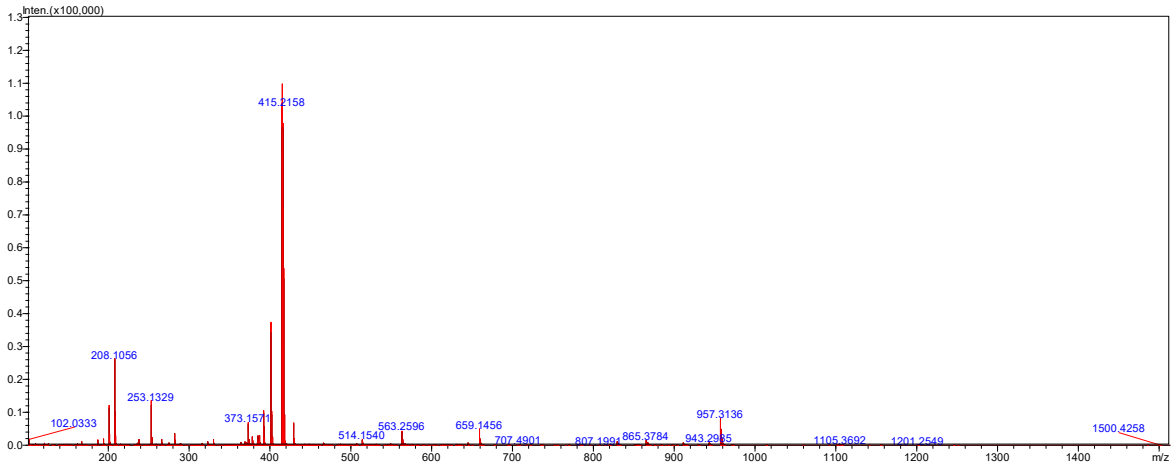

Enlarged MS spectrum in the range 325–600 m/z

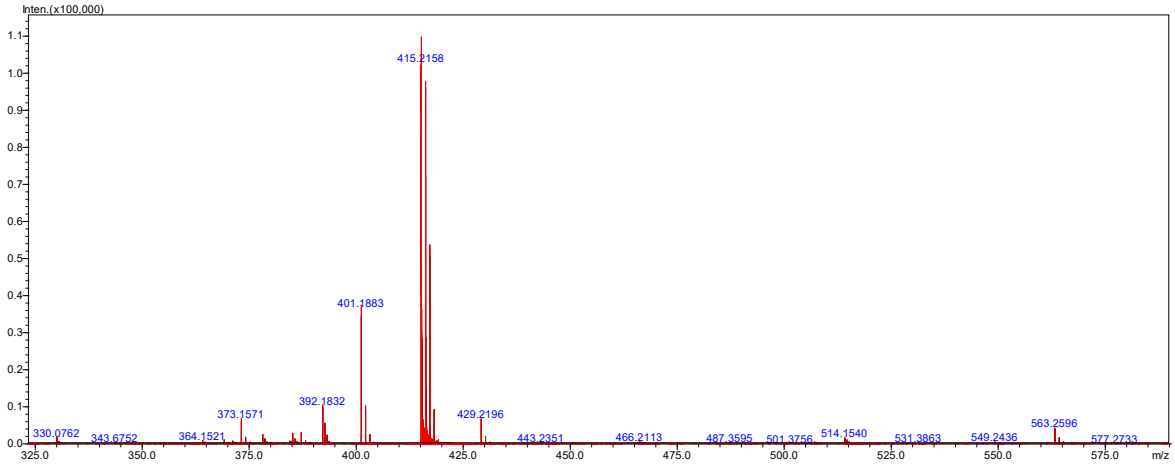

ESI(+) HRMS mass spectrum of **4N2Si** product dissolved in methanol solution.

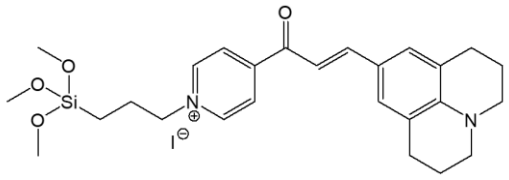

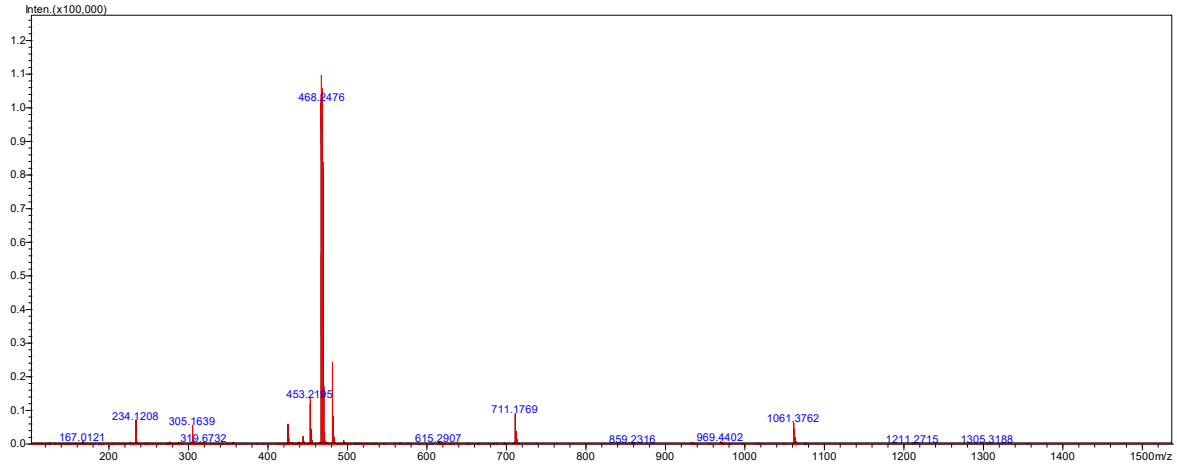

Enlarged MS spectrum in the range 375–750 m/z

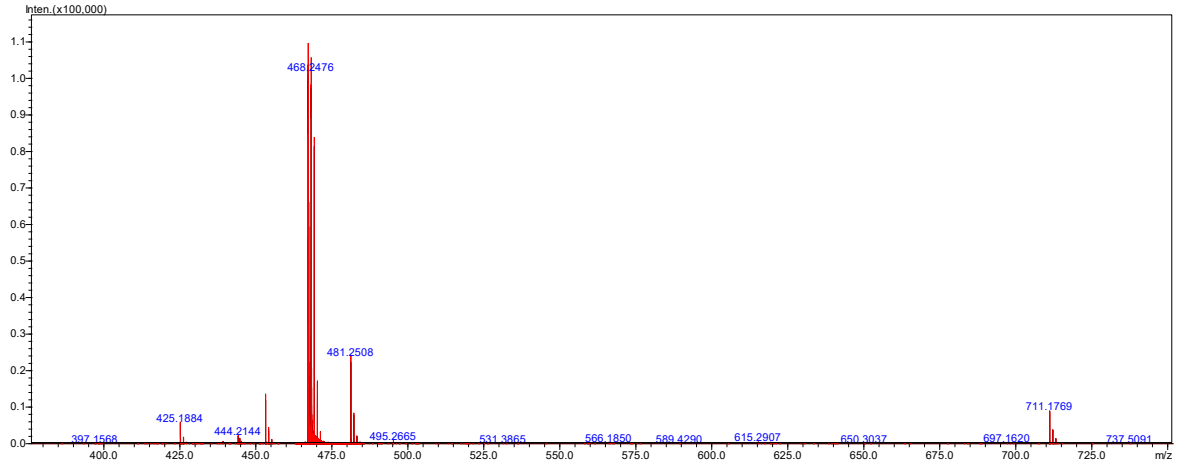

ESI(+) HRMS mass spectrum of **3N2Si** product dissolved in methanol solution.

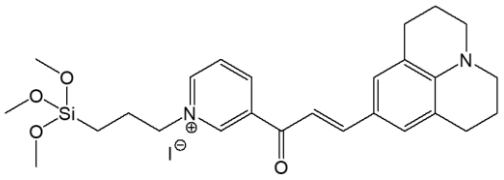

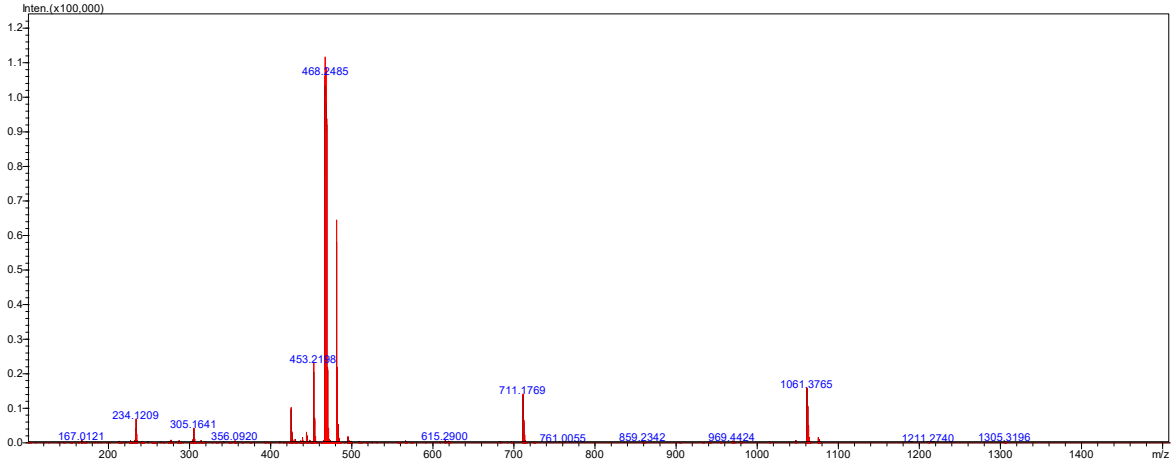

Enlarged MS spectrum in the range 375–625 m/z

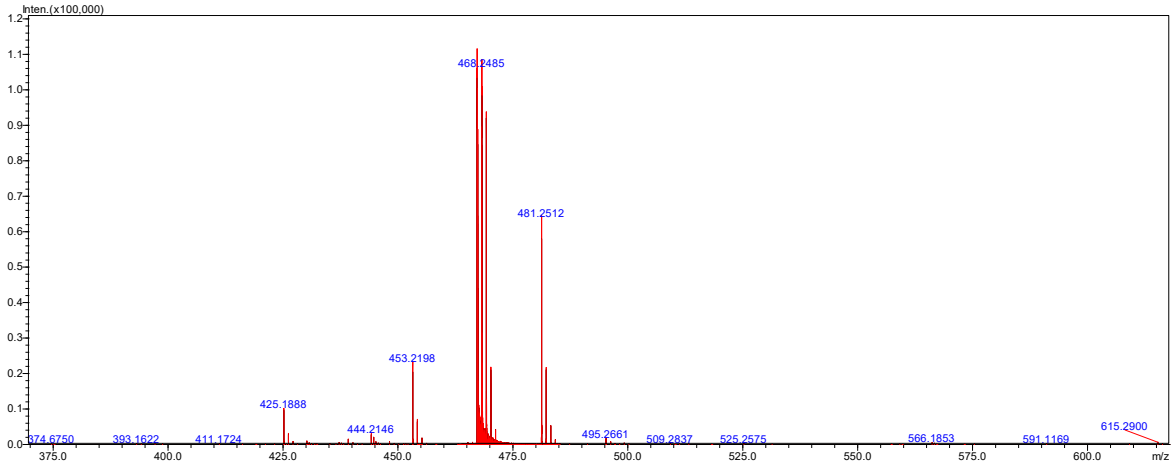

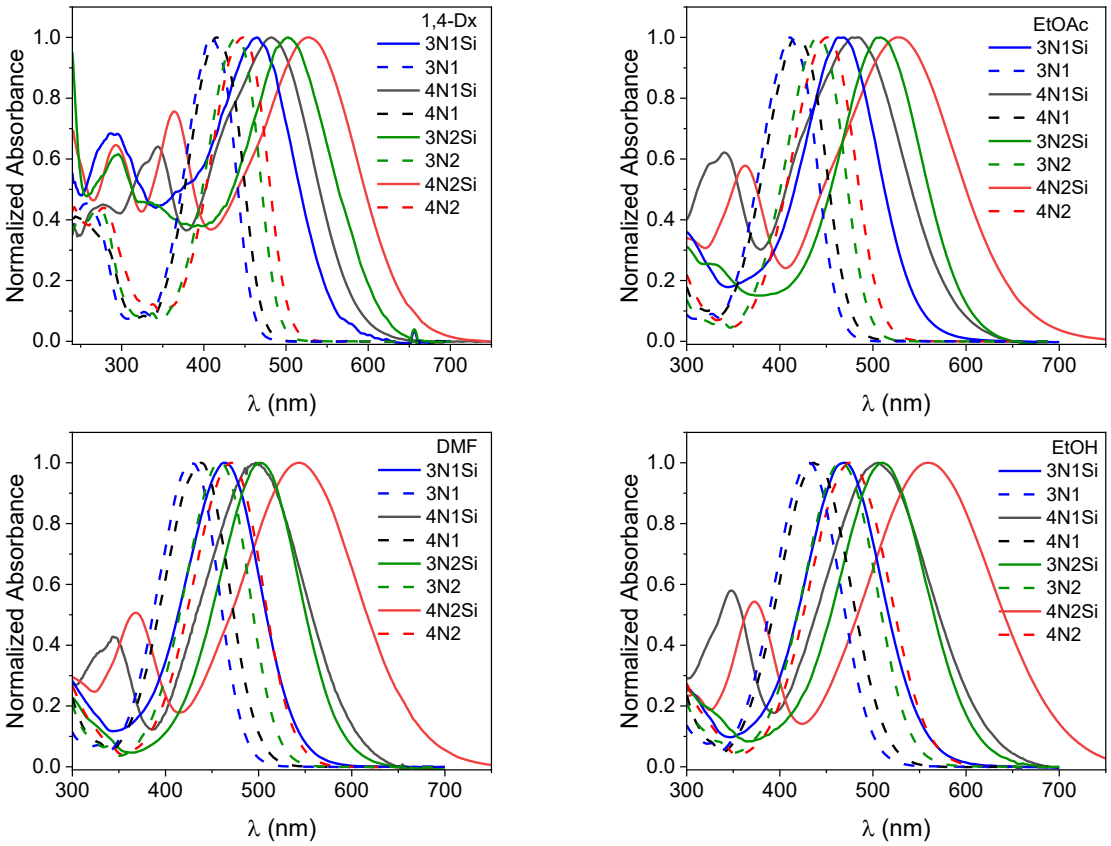

Fig. S1. Comparison of the electronic absorption spectra of the investigated azachalcones and trimethoxysilylazachalcones recorded in four solvents of different polarity (1,4-dioxane, ethyl acetate, DMF, and ethanol).

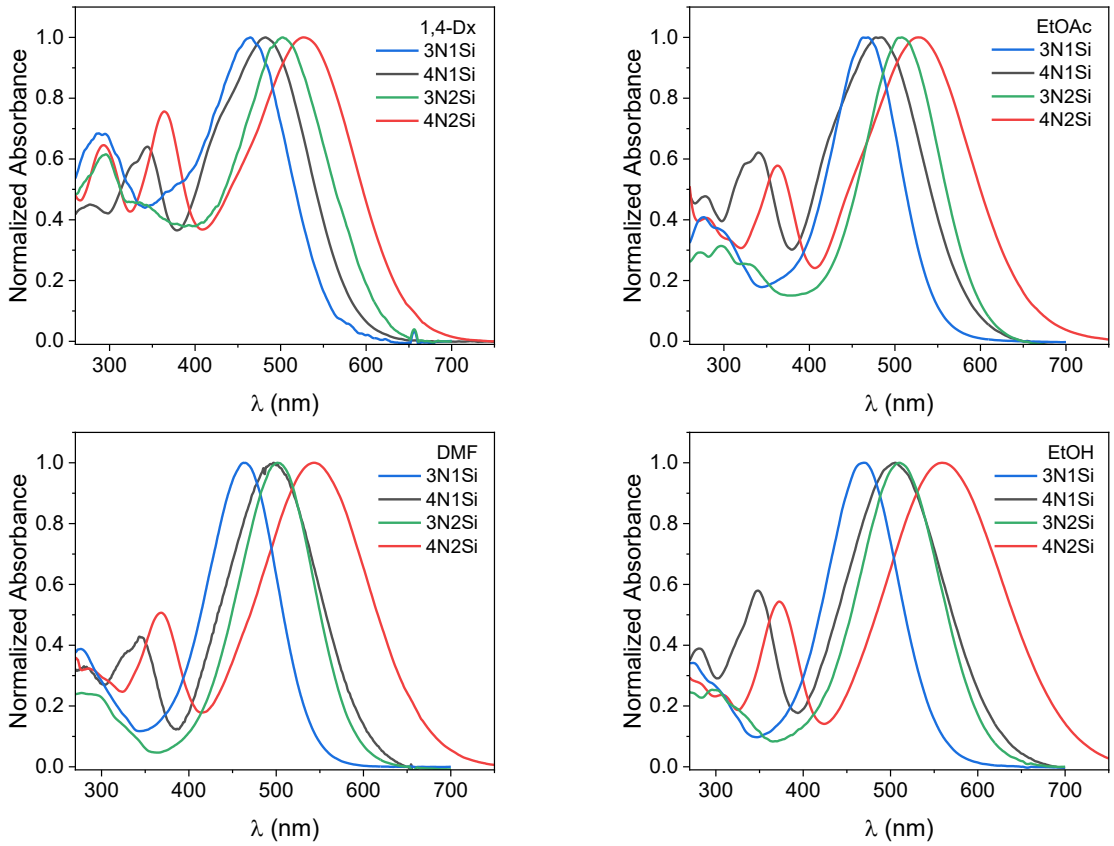

Fig. S2. Electronic absorption spectra of the four investigated trimethoxysilylazachalcones recorded in solvents of different polarity (1,4-dioxane, ethyl acetate, DMF, and ethanol). Each panel displays all four compounds measured in a given solvent, illustrating the influence of solvent environment on their electronic transitions and ICT-related spectral characteristics.

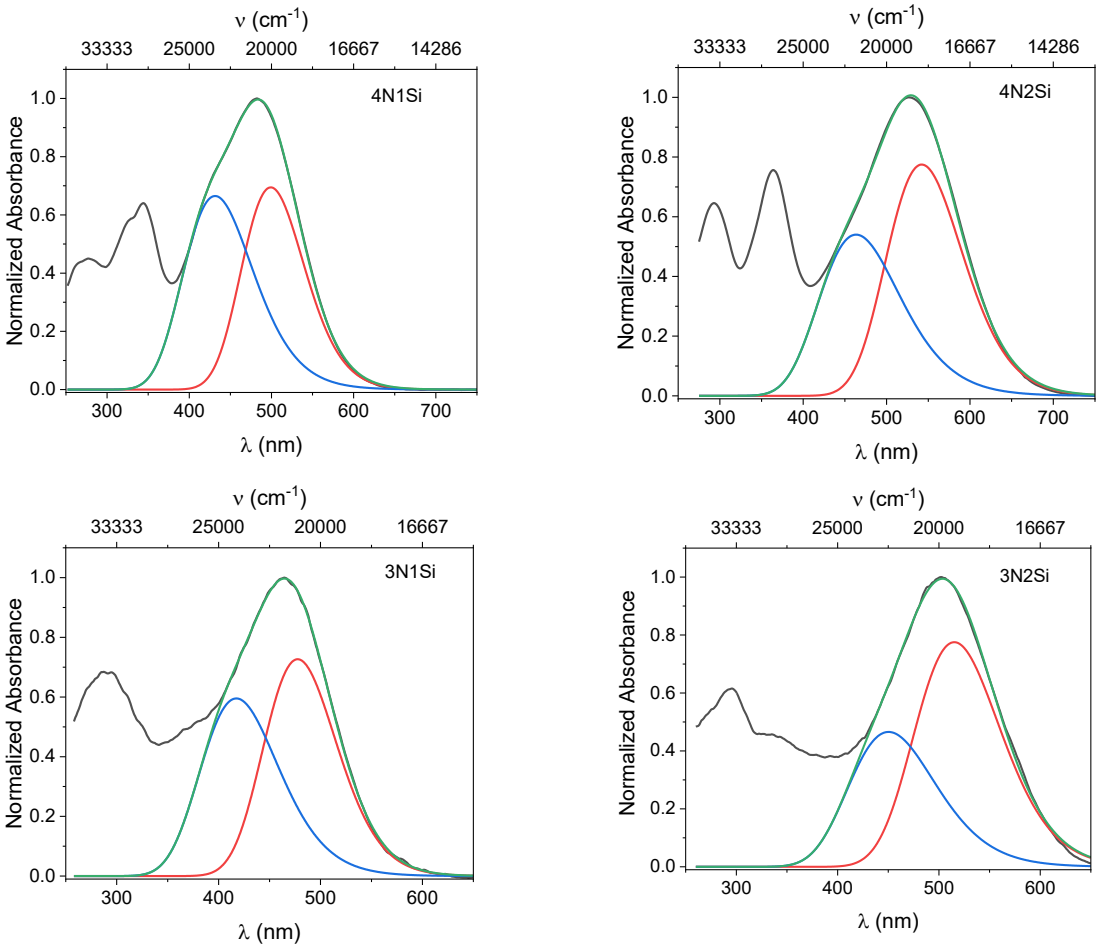

Fig. S3. Distribution of the long-wavelength absorption band of the trimethoxysilylazachalcones in 1,4-Dx.

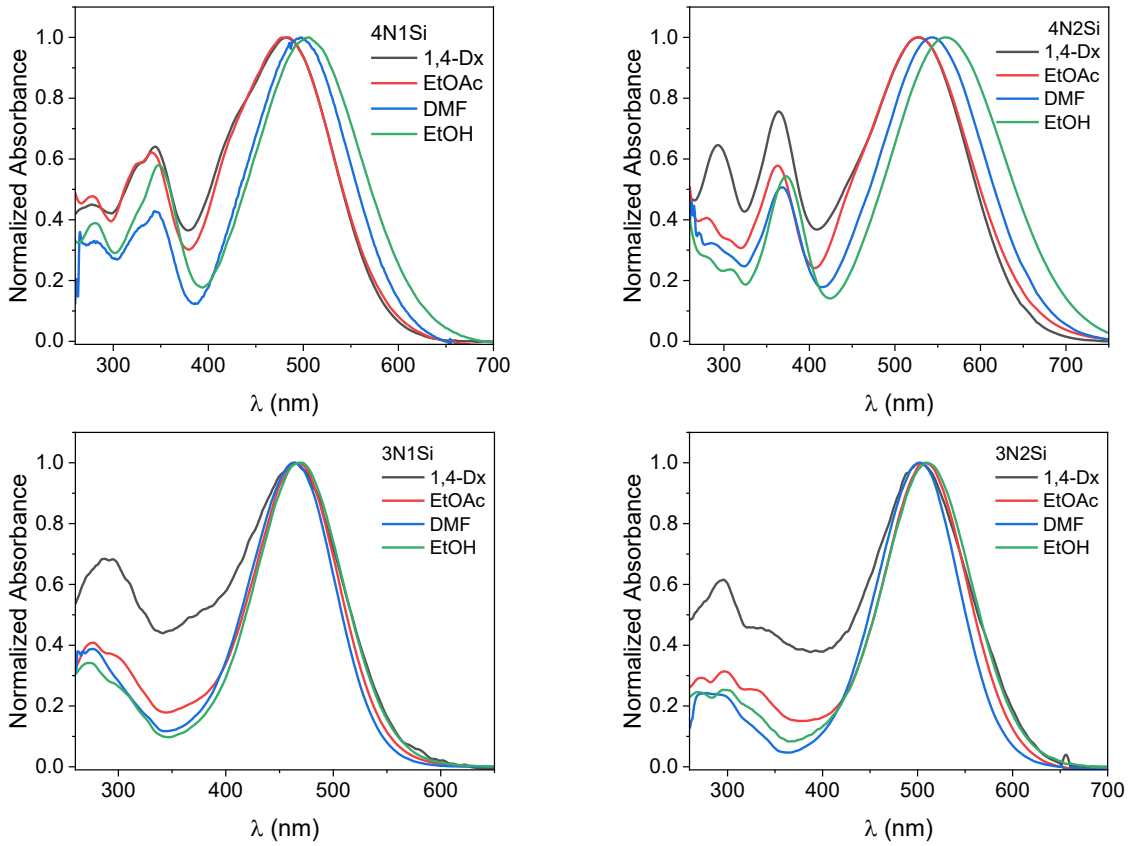

Fig. S4. Influence of solvent polarity on the electronic absorption behaviour of the four trimethoxysilylazachalcones. Each plot corresponds to a different solvent: 1,4-dioxane, ethyl acetate, DMF, or ethanol; and presents the absorption spectra of all four compounds. This representation highlights solvent-dependent variations in their spectral profiles and ICT-related optical responses.

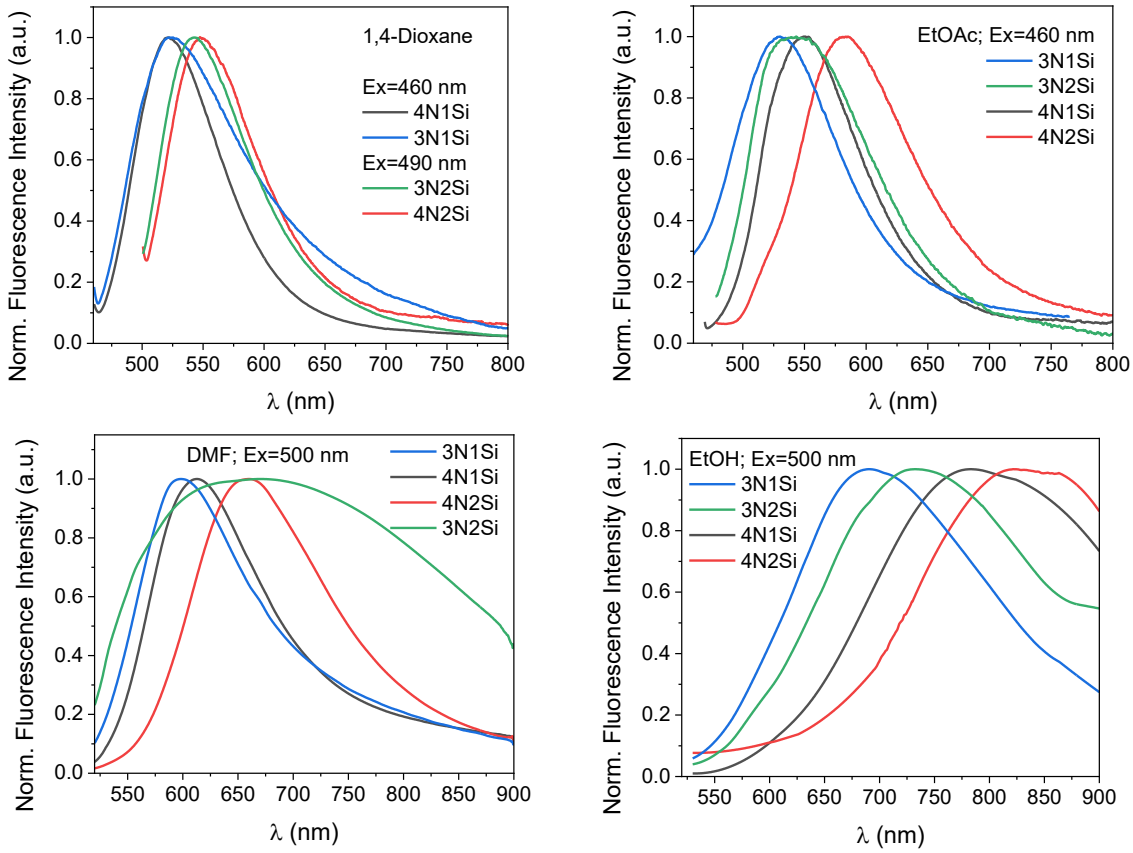

Fig. S5. Effect of the trimethoxysilylazachalcones structure on their fluorescence spectra in solvents of different polarity (1,4-dioxane, ethyl acetate, DMF, and ethanol). Each panel presents the fluorescence spectra of all four compounds measured in a specific solvent, with the excitation wavelength indicated for each panel.

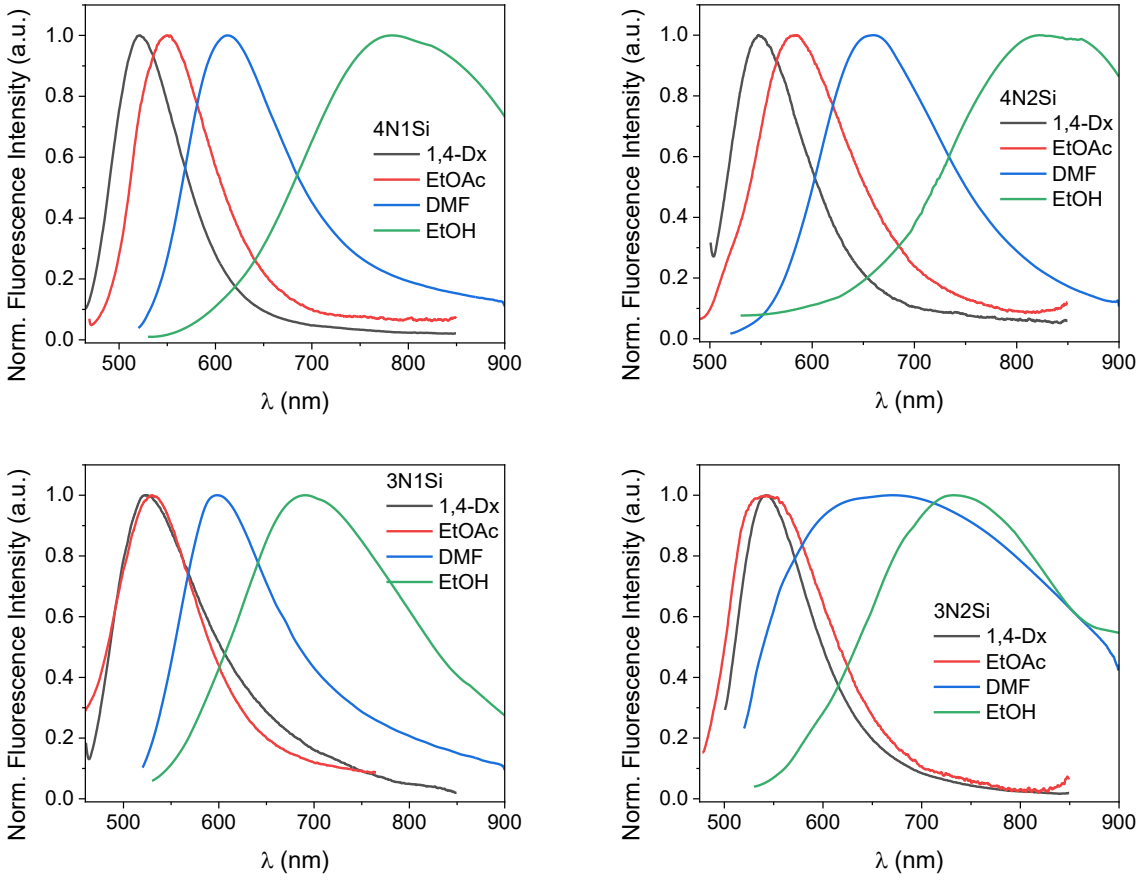

Fig. S6. Effect of solvent polarity on the fluorescence spectra of the trimethoxysilylazachalcones. Each panel shows a single compound measured in four different solvents (1,4-dioxane, ethyl acetate, DMF, and ethanol), with the excitation wavelength as indicated in Figure S5.

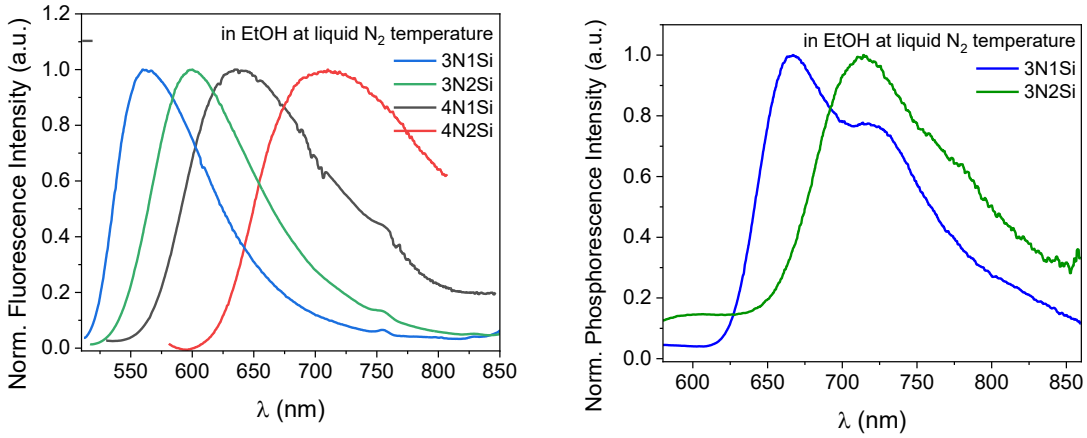

Fig. S7. Fluorescence (left) and phosphorescence (right) spectra of the trimethoxysilylazachalcones in EtOH at liquid nitrogen temperature. Excitation wavelength 500 nm for 4N1Si, 3N1Si and 3N2Si, and 560 nm for 4N2Si.

Table S1. The basic spectroscopic parameters of the tested trimethoxysilylazachalcones, i.e., absorption maxima of the long-wavelength band (λ_{max}^{Ab}), maximum extinction coefficient (ε), fluorescence maxima (λ_{max}^{Fl}) and Stokes shift ($\Delta\nu^{SS}$) in different solvents.

Solvent	λ_{max}^{Ab} (nm)	ε (10^4 $M^{-1}cm^{-1}$)	λ_{max}^{Fl} (nm)	$\Delta\nu^{SS}$ (cm^{-1})	λ_{max}^{Ab} (nm)	ε (10^4 $M^{-1}cm^{-1}$)	λ_{max}^{Fl} (nm)	$\Delta\nu^{SS}$ (cm^{-1})
		4N1Si				**4N2Si**		
1,4-Dx	478	-[1)]	522	1763	526	-	547	730
EtOAc	484	2.15	548	2413	528	2.19	585	1845
DMF	497	2.39	613	3808	544	2.25	660	3231
		3N1Si				**3N2Si**		
1,4-Dx	465	-	525	2458	503	-	542	1431
EtOAc	464	2.42	530	2684	509	2.61	543	1230
DMF	464	2.89	598	4829	502	2.93	670	4995

[1)] Due to very poor solubility, the maximum extinction coefficient was not determined.

Table S2. Computed electronic structure properties of precursors 4N1, 4N2, 3N1, 3N2. Calculated one-photon excitation energy (ΔE^{1PA}), one-photon absorption wavelength (λ^{1PA}), oscillator strength (*f*), Ciofini's charge transfer parameter D^{CT}, charge transfered Q^{CT}, and molecular orbitals involved to this transition.

Transition	ΔE^{1PA} (eV)	λ^{1PA} (nm)	*F*	D^{CT} (Å)	Q^{CT} (a.u.)	Dominant molecular orbitals
			4N1			
$S_0 \rightarrow S_1$	3.151	393	1.120	3.76	0.734	HOMO → LUMO
$S_0 \rightarrow S_2$	3.800	326	0.004	1.07	0.778	HOMO−4 → LUMO
$S_0 \rightarrow S_3$	4.460	278	0.033	0.93	0.526	HOMO → LUMO+5
			4N2			
$S_0 \rightarrow S_1$	2.996	414	1.086	3.75	0.756	HOMO → LUMO
$S_0 \rightarrow S_2$	3.805	326	0.002	1.11	0.787	HOMO−4 → LUMO
$S_0 \rightarrow S_3$	4.246	292	0.010	2.29	0.414	HOMO−1 → LUMO
			3N1			
$S_0 \rightarrow S_1$	3.219	385	1.159	3.68	0.727	HOMO → LUMO
$S_0 \rightarrow S_2$	3.839	323	0.003	1.16	0.784	HOMO−2 → LUMO
$S_0 \rightarrow S_3$	4.466	278	0.042	0.75	0.533	HOMO → LUMO+5
			3N2			
$S_0 \rightarrow S_1$	3.065	405	1.110	3.68	0.751	HOMO → LUMO
$S_0 \rightarrow S_2$	3.846	322	0.003	1.19	0.792	HOMO−3 → LUMO
$S_0 \rightarrow S_3$	4.261	291	0.016	1.82	0.417	HOMO−1 → LUMO

Table S3. Computed electronic structure properties of compounds 4N1Si, 4N2Si, 3N1Si, 3N2. Calculated one-photon excitation energy (ΔE^{1PA}), one-photon absorption wavelength (λ^{1PA}), oscillator strength (*f*), Ciofini's charge transfer parameter D^{CT}, charge transfered Q^{CT}, and molecular orbitals involved to this transition.

Transition	ΔE^{1PA} (eV)	λ^{1PA} (nm)	*f*	D^{CT} (Å)	Q^{CT} (a.u.)	Dominant molecular orbitals
			4N1Si			
$S_0 \rightarrow S_1$	2.886	430	1.041	4.18	0.792	HOMO → LUMO
$S_0 \rightarrow S_2$	3.709	334	0.003	0.93	0.801	HOMO−3 → LUMO
$S_0 \rightarrow S_3$	4.146	299	0.236	4.98	0.902	HOMO → LUMO+1
			4N2Si			
$S_0 \rightarrow S_1$	2.714	457	1.012	4.18	0.814	HOMO → LUMO
$S_0 \rightarrow S_2$	3.701	335	0.003	0.96	0.811	HOMO−3 → LUMO
$S_0 \rightarrow S_3$	3.949	314	0.193	4.86	0.915	HOMO → LUMO+1
			3N1Si			
$S_0 \rightarrow S_1$	3.038	408	1.188	3.82	0.745	HOMO → LUMO
$S_0 \rightarrow S_2$	3.883	319	0.002	1.01	0.800	HOMO−3 → LUMO
$S_0 \rightarrow S_3$	3.990	311	0.048	5.31	1.235	HOMO → LUMO+1
			3N2Si			
$S_0 \rightarrow S_1$	2.881	430	1.164	3.82	0.761	HOMO → LUMO
$S_0 \rightarrow S_2$	3.804	326	0.040	5.29	1.273	HOMO → LUMO+1
$S_0 \rightarrow S_3$	3.890	319	0.003	1.05	0.810	HOMO−3 → LUMO

HOMO LUMO

Fig. S8. Compound 4N1, frontier molecular orbitals (plotted with the same contour value (0.02)).

HOMO LUMO

Fig. S9. Compound 4N2, frontier molecular orbitals (plotted with the same contour value (0.02)).

HOMO LUMO

Fig. S10. Compound 3N1, frontier molecular orbitals (plotted with the same contour value (0.02)).

HOMO LUMO

Fig. S11. Compound 3N2, frontier molecular orbitals (plotted with the same contour value (0.02)).

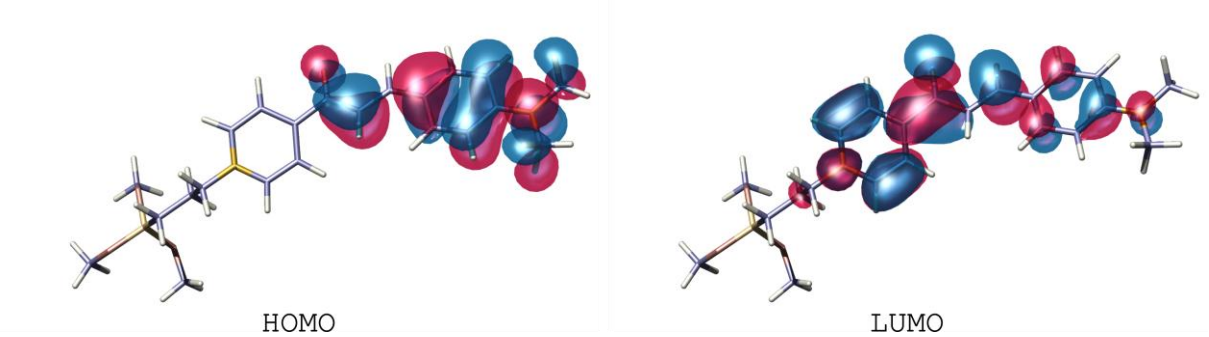

Fig. S12. Compound 4N1Si, frontier molecular orbitals (plotted with the same contour value (0.02)).

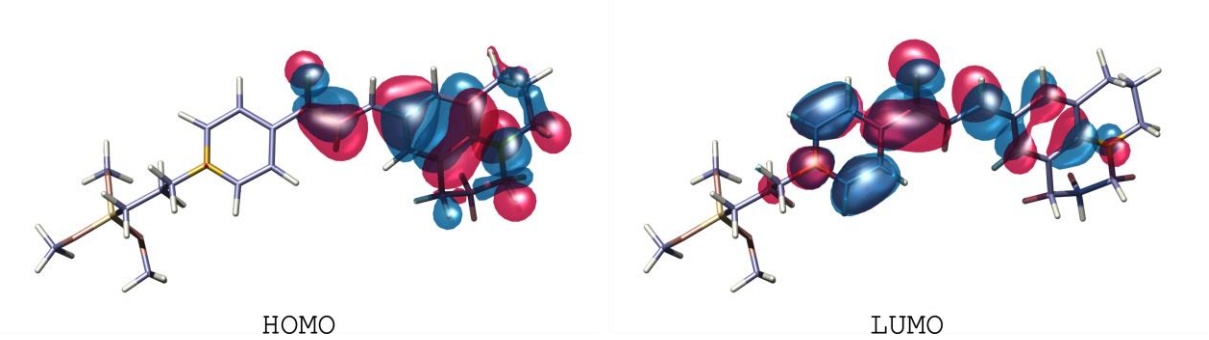

Fig. S13. Compound 4N2Si, frontier molecular orbitals (plotted with the same contour value (0.02)).

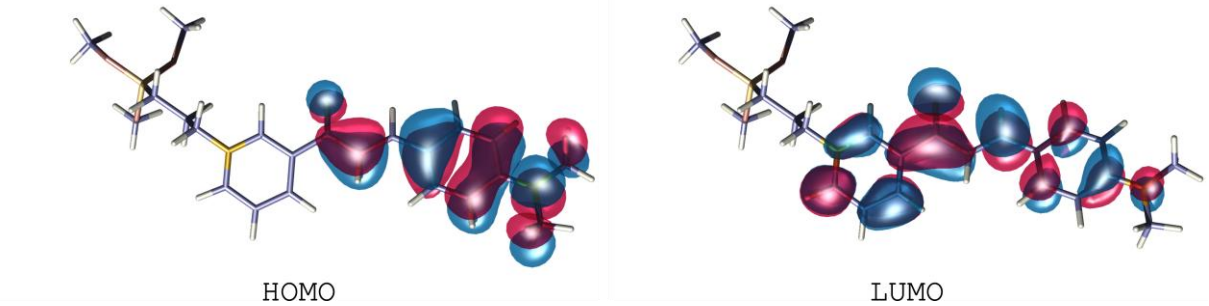

Fig. S14. Compound 3N1Si, frontier molecular orbitals (plotted with the same contour value (0.02)).

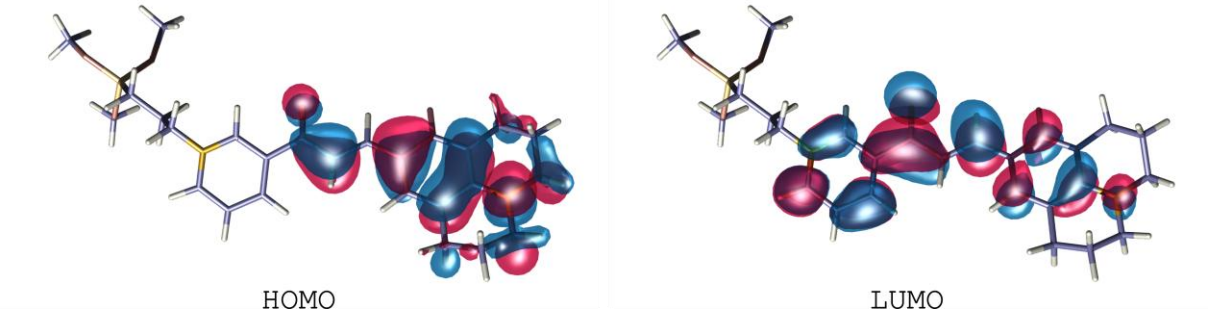

Fig. S15. Compound 3N2Si, frontier molecular orbitals (plotted with the same contour value (0.02)).

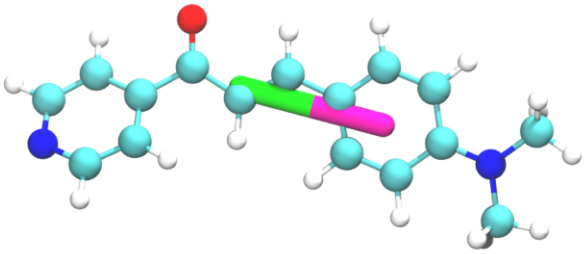

$S_0 \rightarrow S_1$

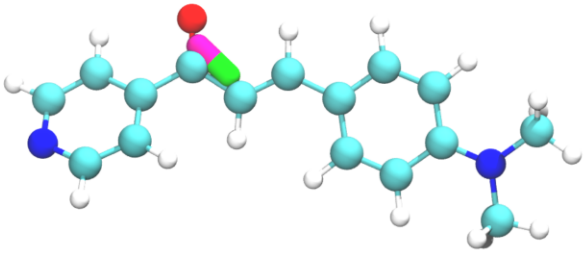

$S_0 \rightarrow S_2$

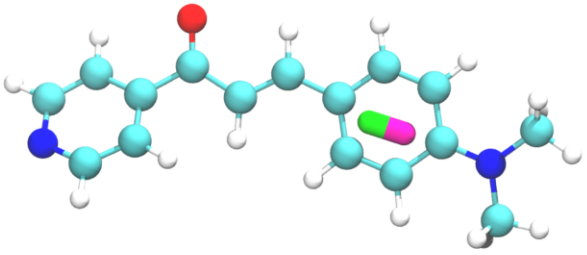

$S_0 \rightarrow S_3$

Fig. S16. Compound 4N1, graphical representation of Ciofini's charge transfer parameter D^{CT}. Magenta colour represents depletion of the charge density, Green colour represents increase of the density.

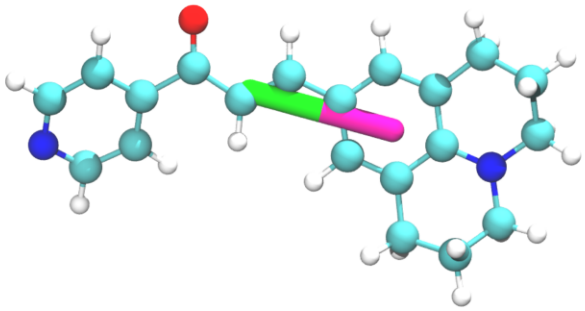

$S_0 \rightarrow S_1$

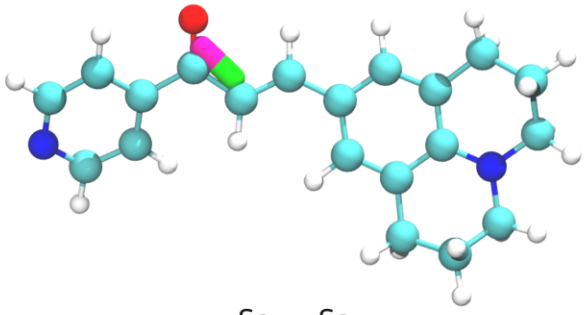

$S_0 \rightarrow S_2$

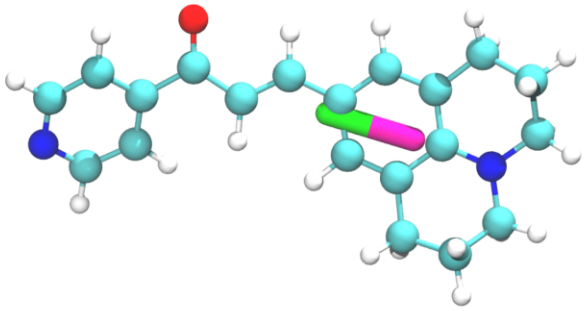

$S_0 \rightarrow S_3$

Fig. S17. Compound 4N2, graphical representation of Ciofini's charge transfer parameter D^{CT}. Magenta colour represents depletion of the charge density, Green colour represents increase of the density.

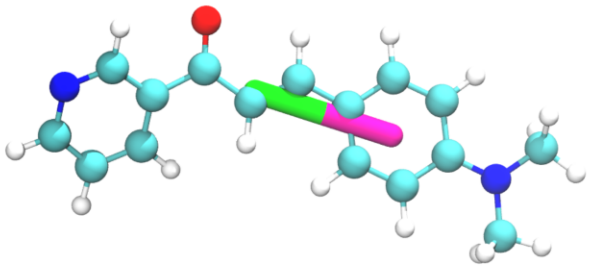

$S_0 \rightarrow S_1$

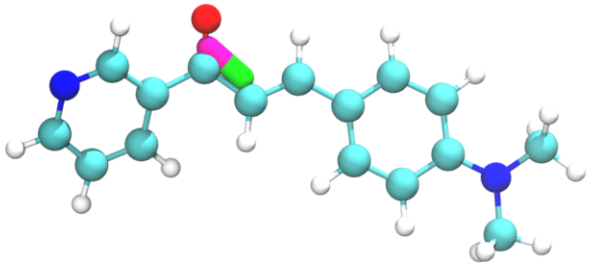

$S_0 \rightarrow S_2$

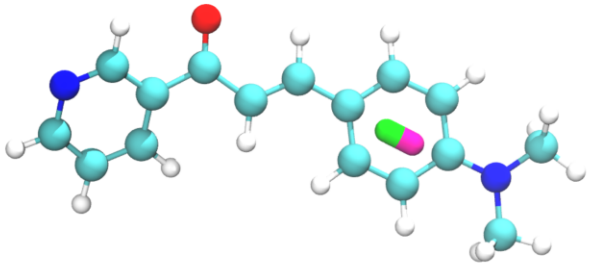

$S_0 \rightarrow S_3$

Fig. S18. Compound 3N1, graphical representation of Ciofini's charge transfer parameter D^{CT}. Magenta colour represents depletion of the charge density, Green colour represents increase of the density.

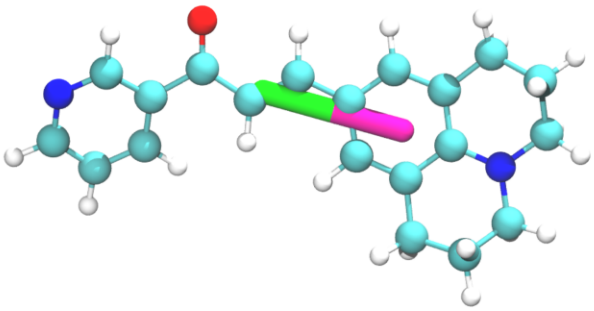

$S_0 \rightarrow S_1$

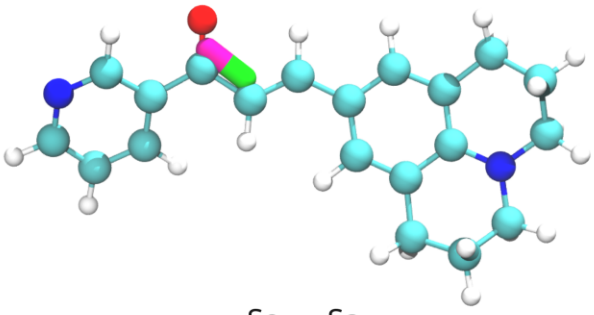

$S_0 \rightarrow S_2$

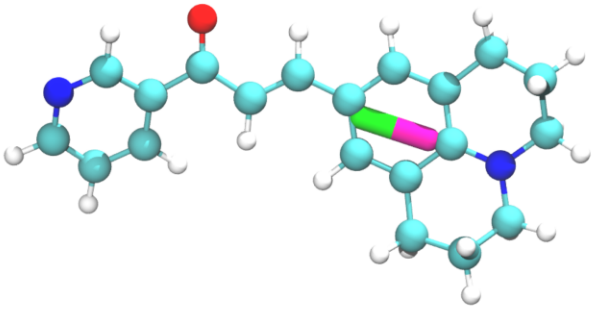

$S_0 \rightarrow S_3$

Fig. S19. Compound 3N2, graphical representation of Ciofini's charge transfer parameter D^{CT}. Magenta colour represents depletion of the charge density, Green colour represents increase of the density.

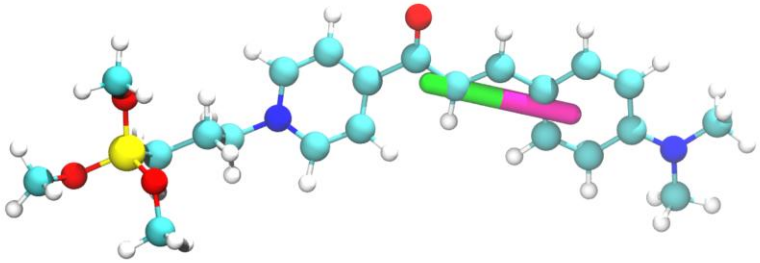

$S_0 \rightarrow S_1$

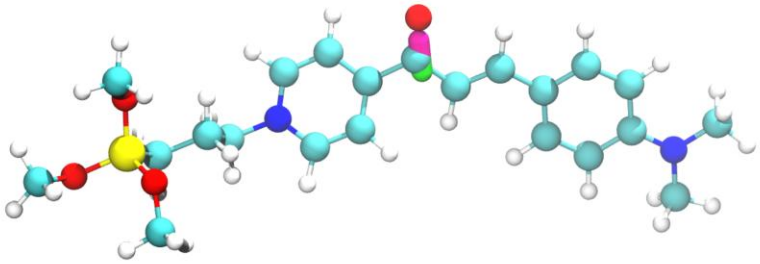

$S_0 \rightarrow S_2$

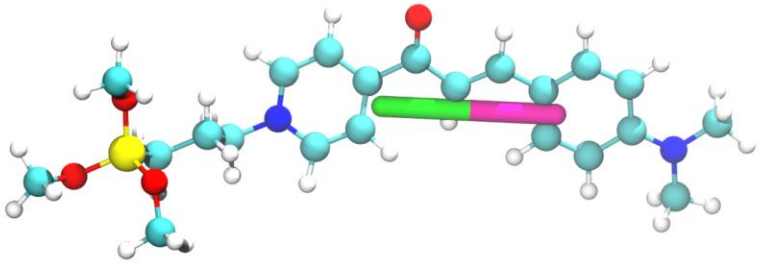

$S_0 \rightarrow S_3$

Fig. S20. Compound 4N1Si, graphical representation of Ciofini's charge transfer parameter D^{CT}. Magenta colour represents depletion of the charge density, Green colour represents increase of the density.

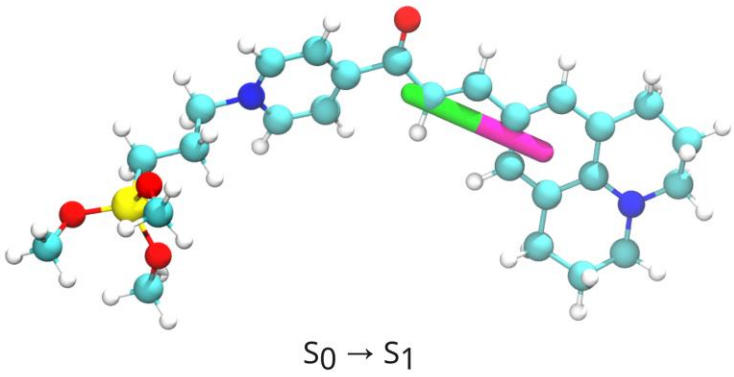

$S_0 \rightarrow S_1$

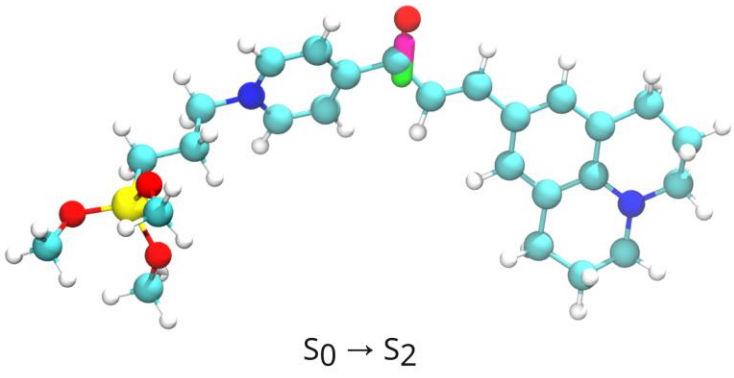

$S_0 \rightarrow S_2$

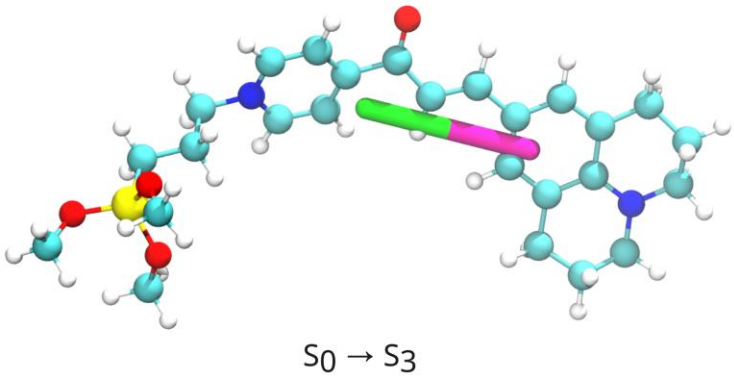

$S_0 \rightarrow S_3$

Fig. S21. Compound 4N2Si, graphical representation of Ciofini's charge transfer parameter D^{CT}. Magenta colour represents depletion of the density, green colour represents increase of the density.

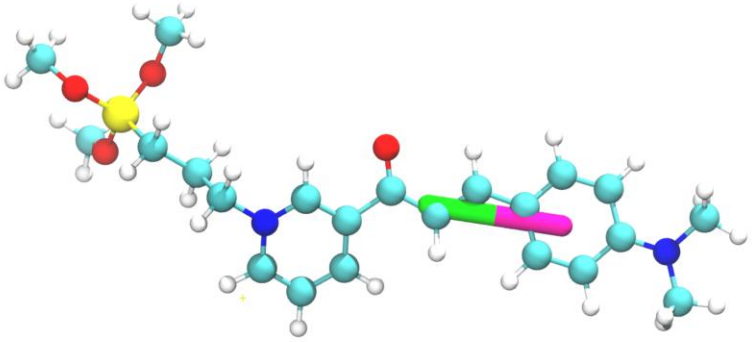

$S_0 \rightarrow S_1$

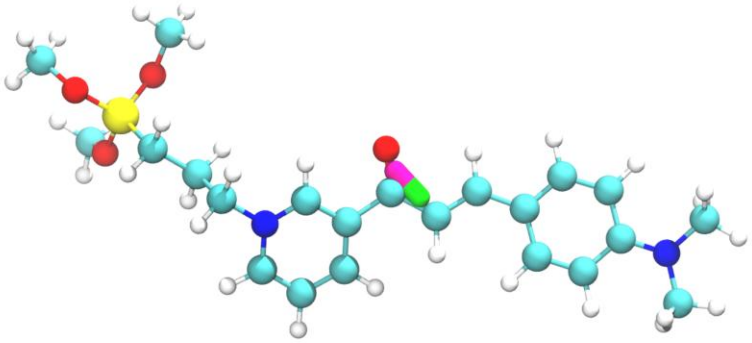

$S_0 \rightarrow S_2$

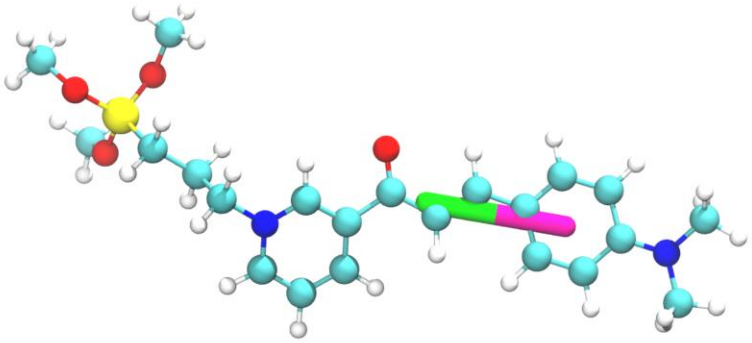

$S_0 \rightarrow S_3$

Fig. S22. Compound 3N1Si, graphical representation of Ciofini's charge transfer parameter D^{CT}. Green colour represents depletion of the density, magenta colour represents increase of the density.

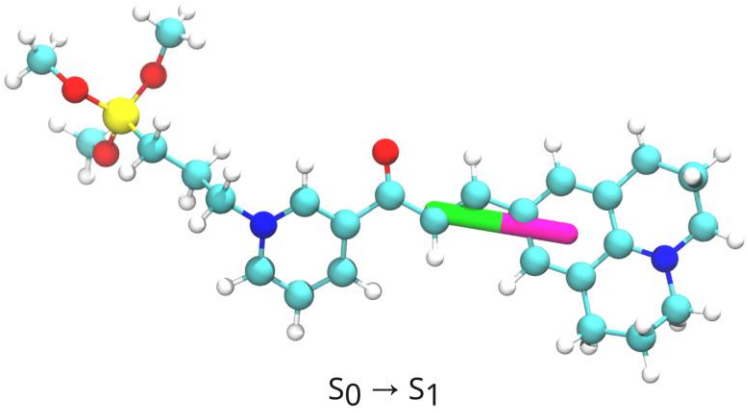

$S_0 \rightarrow S_1$

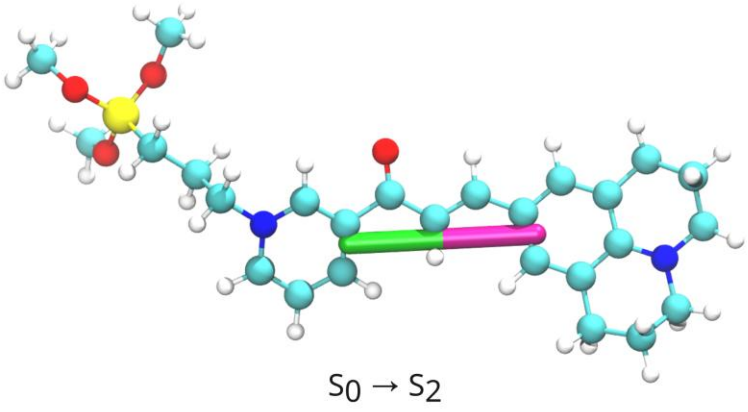

$S_0 \rightarrow S_2$

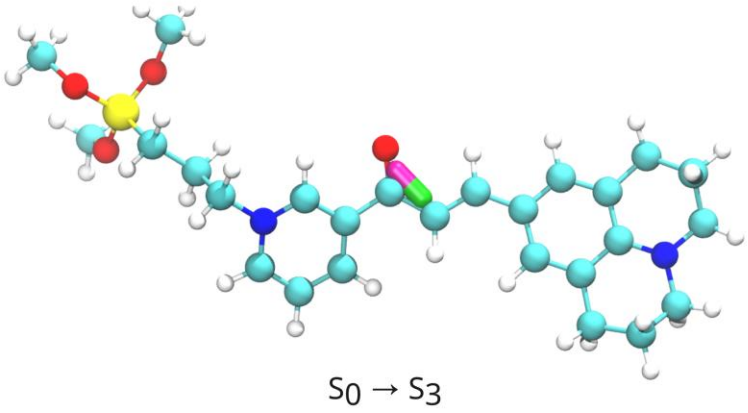

$S_0 \rightarrow S_3$

Fig. S23. Compound 3N2Si, graphical representation of Ciofini's charge transfer parameter D^{CT}. Magenta colour represents depletion of the charge density, Green colour represents increase of the charge density.

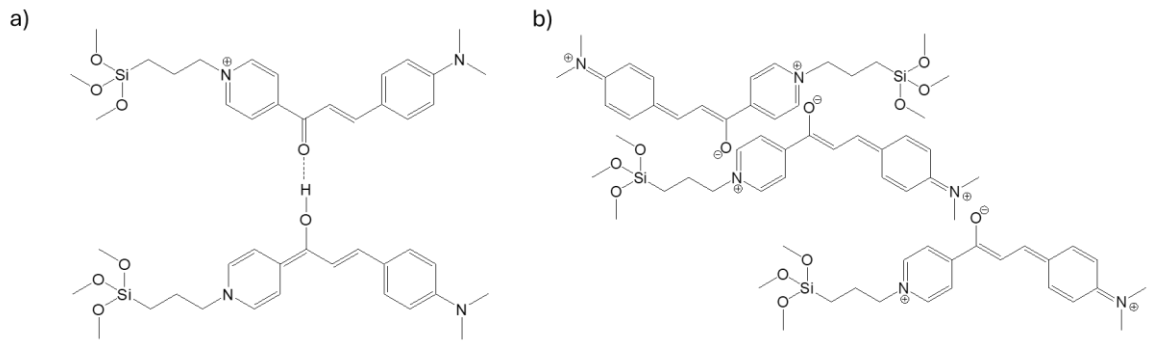

Fig. S24. Proposed interaction mechanisms: (a) formation of hydrogen bonds, and (b) electrostatic interaction involving the zwitterionic mesomeric form of the chalcone molecule.

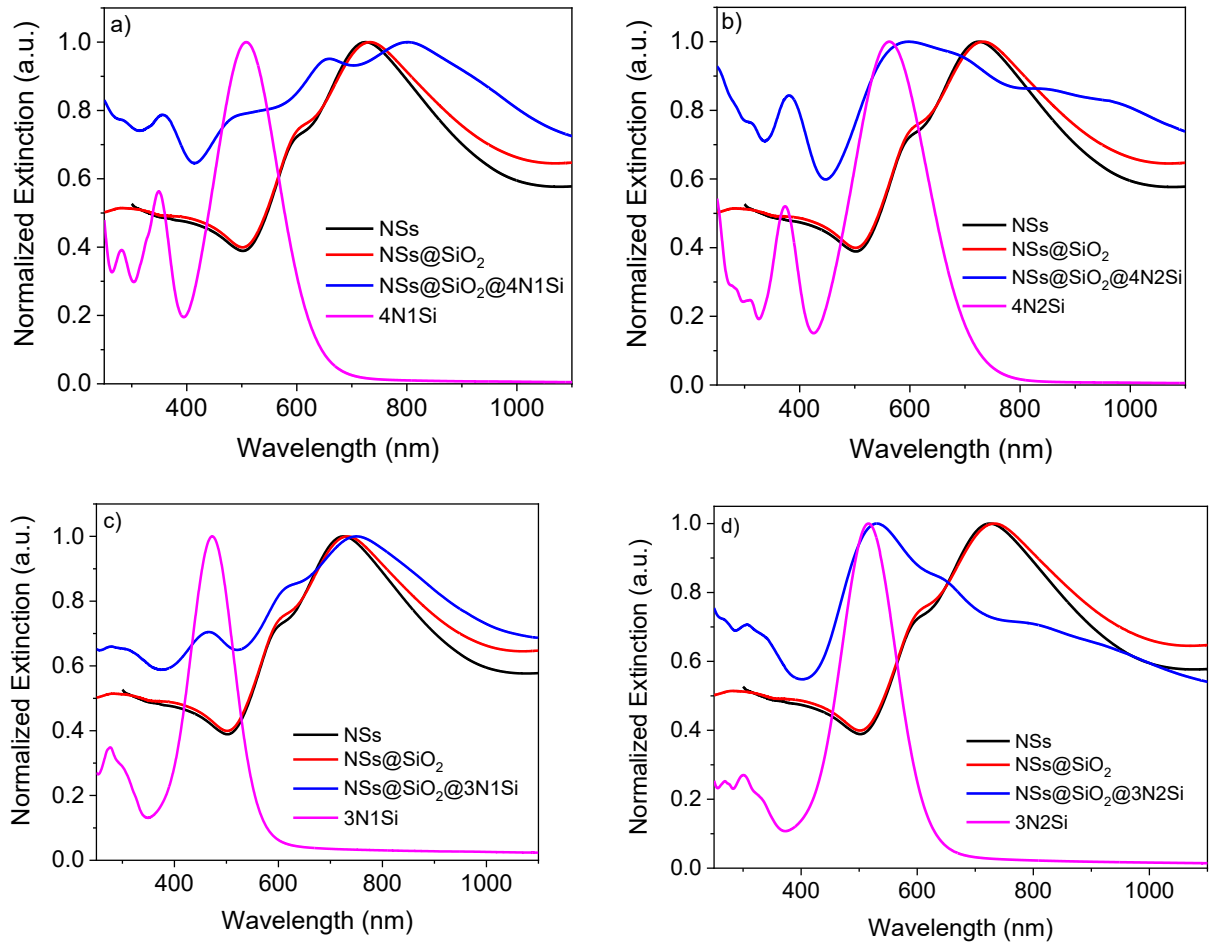

Fig. S25. Normalized extinction spectra for NSs in water, NSs@SiO_2 in ethanol, NSs@SiO_2 with: 4N1Si (a), 4N2Si (b), 3N1Si (c), 3N2Si (d) in ethanol.

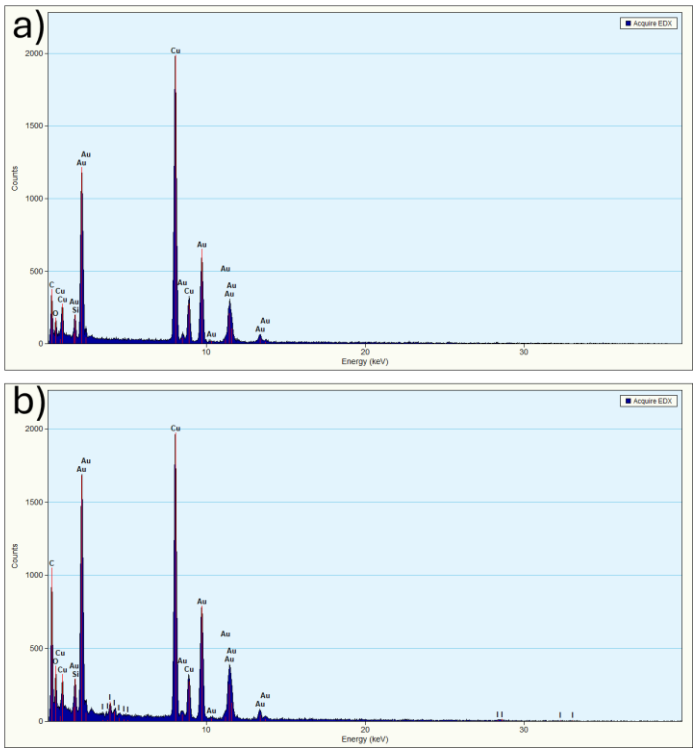

Fig. S26. Representative EDX spectra obratned for a) NSs@SiO_2 and b) NSs@SiO_2@4N1Si.

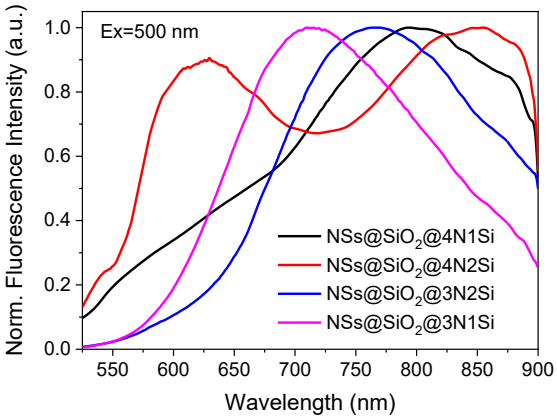

Fig. S27. Fluorescence spectra of NSs with silica and trimethoxysilylazachalcones in EtOH excited at 500 nm.

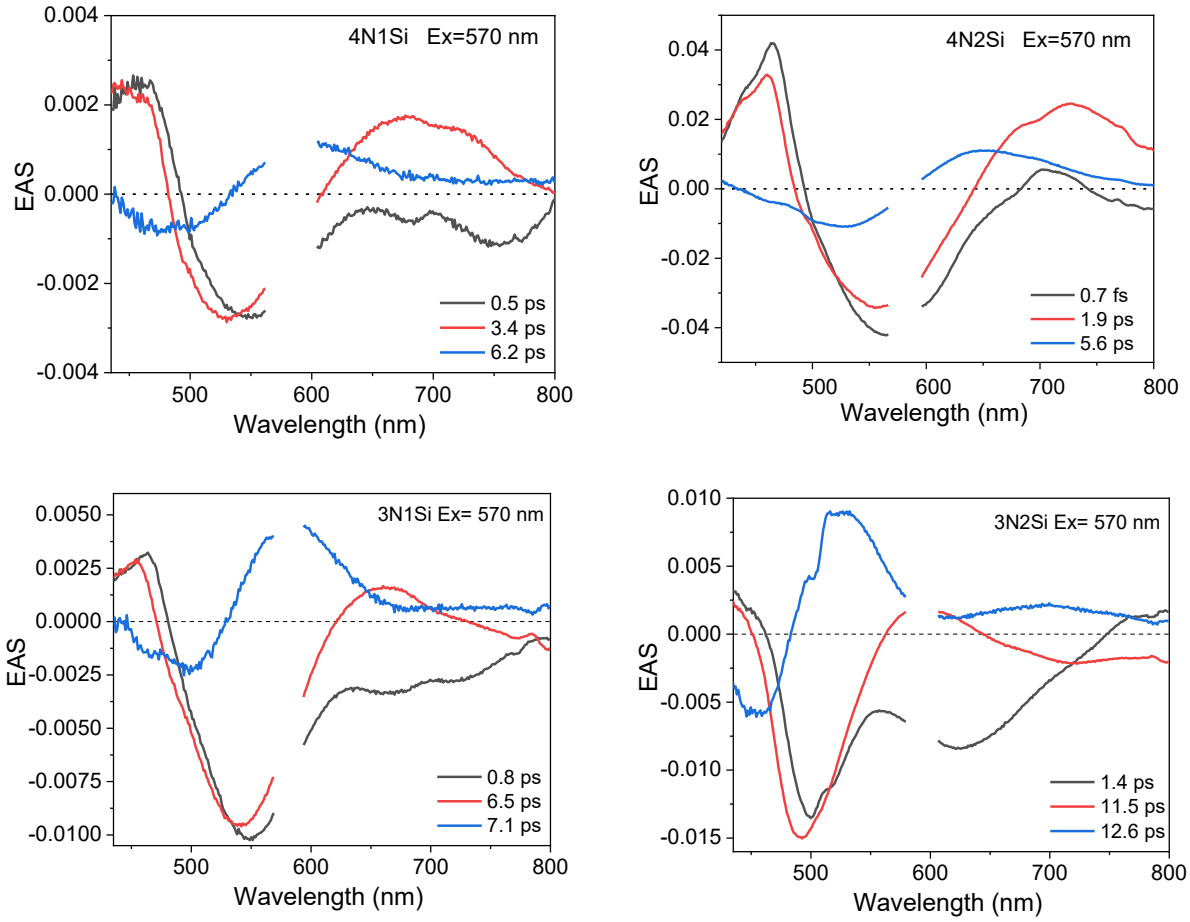

Fig. S28. Evolution associated difference spectra obtained from sequential three-compartment model for: 4N1Si, 4N2Si, 3N1Si, 3N2Si.

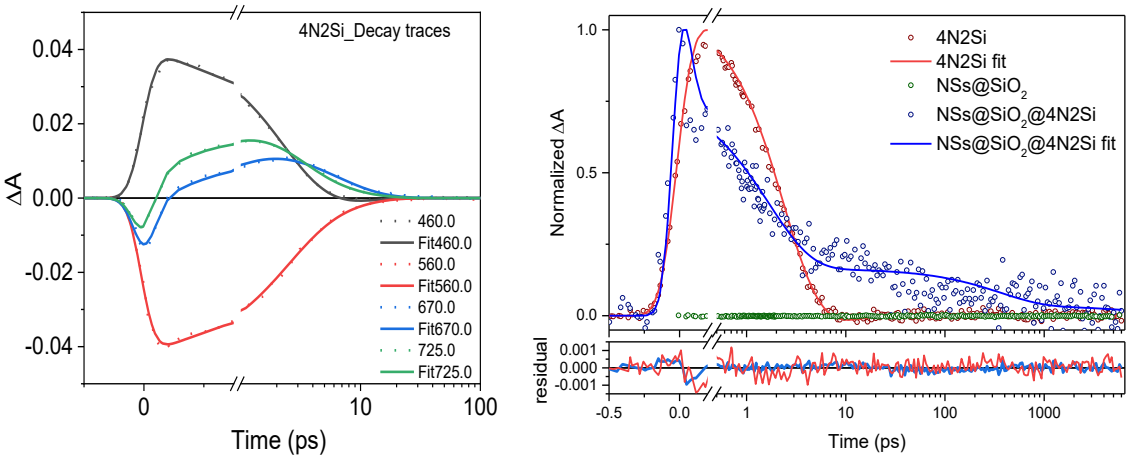

Fig. S29. Left: The temporal absorption profiles recorded at 460, 560, 670, and 725 nm for 4N2Si sample obrained after sequential three exponential model fit. Right: Time course of normalized transient absorbance recorded at 450 nm for 4N2Si (red) and NSs@SiO_2@4N2Si (blue). The reference signal from bare NSs is plotted in green. Points - experimental data, lines are plotted based on target model.